Applied Catalysis B: Environmental 239 (2018) 68–76

Contents lists available at ScienceDirect

Applied Catalysis B: Environmental

journal homepage: www.elsevier.com/locate/apcatb

On the selectivity of CO_2 photoreduction towards CH_4 using Pt/TiO_2 catalysts supported on mesoporous silica

Minoo Tasbihi[a,*], Fernando Fresno[b,*], Ulla Simon[c], Ignacio J. Villar-García[b], Virginia Pérez-Dieste[d], Carlos Escudero[d], Víctor A. de la Peña O'Shea[b]

[a] Department of Chemistry, Technical University Berlin, Straße des 17. Juni 124, 10623 Berlin, Germany
[b] Photoactivated Processes Unit, IMDEA Energy Institute, Parque Tecnológico de Móstoles, Avda. Ramón de la Sagra 3, 28935 Móstoles, Madrid, Spain
[c] Fachgebiet Keramische Werkstoffe/Chair of Advanced Ceramic Materials, Institut für Werkstoffwissenschaften und-technologien, Fakultät III, Technische Universität Berlin, Hardenbergstr. 40, 10623 Berlin, Germany
[d] ALBA Synchrotron Light Source, Carrer de la Llum 2–26, 08290 Cerdanyola del Vallès, Barcelona, Spain

ARTICLE INFO

Keywords:
CO_2 reduction
Artificial photosynthesis
Pt/TiO_2
Ordered mesoporous silica
NAP-XPS

ABSTRACT

Pt/TiO_2 and Pt/TiO_2-COK-12 photocatalysts have been prepared by a deposition-precipitation method and characterized by means of X-ray diffraction (XRD), N_2 adsorption isotherms, transmission electron microscopy (TEM), UV–vis diffuse reflectance spectroscopy (UV–vis DRS) and inductively coupled plasma optical emission spectrometry (ICP-OES). The photocatalytic activity of as-prepared photocatalyst was tested for the photocatalytic reduction of CO_2 under UV light in a continuous flow gas-phase photoreactor. CH_4 and CO were detected as major carbon products for all photocatalysts, with minor amounts of CH_3OH. Carbon monoxide is the main product obtained over TiO_2 regardless of the presence of COK-12 as a mesoporous support, whereas Pt leads to CO_2 reduction towards CH_4 formation, with a selectivity that reaches *ca.* 100% with optimum loading. Supporting the Pt/TiO_2 catalysts on COK-12 preserves the selectivity of the reaction towards CH_4 and further improves the overall activity of the Pt/TiO_2 materials. After-reaction attenuated total reflection infrared spectroscopy (ATR-IR) and *in-situ* near ambient pressure X-ray photoelectron spectroscopy (NAP-XPS) have been employed to identify reaction intermediates and used to explain the observed selectivity trends.

1. Introduction

Greenhouse gases such as carbon dioxide (CO_2), methane (CH_4), nitrous oxide (N_2O), ozone (O_3) and chlorofluorocarbons (CFCs) are the primary cause of global warming. Since 1750, beginning of the Industrial Revolution, human activities have produced a 40% increase in the atmospheric concentration of carbon dioxide, from 280 ppm in 1750 to 400 ppm in 2015 [1]. The amount of CO_2 emitted to the atmosphere can be diminished mainly by three methodologies: i) efficient use of carbon-based energy sources; ii) use of alternative or carbon-free energy sources; and iii) capture of CO_2 by post-treatment technologies and subsequent use for different applications, *e.g.* meat freezing, methanol production, or injection into geological formation for enhanced recovery of fossil fuel products [2,3]. Currently, great research activities have been devoted to CO_2 capture, storage and utilization, among which the photocatalytic reduction of CO_2 into hydrocarbon fuels is considered to be one of the most promising solutions to stabilize the concentration of CO_2 in the atmosphere [4,5]. Inoue et al. showed the possibility to reduce CO_2 photoelectrocatalytically using semiconductor materials as early as 1979 [6]. Since then, the efficient photocatalytic reduction of CO_2 with H_2O has remained one of the most desirable and challenging goals in the research for energy and environment. The photocatalytic reduction of CO_2 is not only attractive due to is potential to remove CO_2 but also because it can promote its conversion into energy-bearing or chemically useful products such as methane (CH_4), methanol (CH_3OH), formaldehyde (HCHO), carbon monoxide (CO), formic acid (HCOOH) and ethylene (C_2H_4) [7].

The photocatalytic reduction of CO_2 is based on the use of electrons and holes produced in a semiconductor (most usually TiO_2), upon irradiation with light of the appropriate energy (UV for TiO_2), to promote reduction and oxidation reactions of molecular species adsorbed on the semiconductor surface. So far, titania (TiO_2) has been the most explored semiconductor for photocatalytic applications due to its outstanding chemical and thermal stability. However, its large band gap and relatively high recombination rate of photoinduced electron-hole pairs still leave room from improvement of its photocatalytic activity [8].

* Corresponding authors.
E-mail addresses: minoo.tasbihi@tu-berlin.de (M. Tasbihi), fernando.fresno@imdea.org (F. Fresno).

https://doi.org/10.1016/j.apcatb.2018.08.003
Received 10 June 2018; Received in revised form 27 July 2018; Accepted 1 August 2018
Available online 02 August 2018
0926-3373/

Particularly for energy applications of photocatalysis, improving the electron-hole separation efficiency and light utilization ability of TiO_2 would make a significant impact. Among other strategies, the modification of TiO_2 through noble metal deposition is widely applied by researchers in the field of photocatalytic CO_2 reduction. Ishitani et al. [9] were the first to systematically study the photoreduction of CO_2 on a series of metal-decorated TiO_2 showing that depositing metals on TiO_2 could enhance the photocatalytic reduction of CO_2 and modify the product distribution. Afterwards, there has been a significant number of works reporting that such co-catalysts loaded on the surface of the semiconductor can serve as electron traps to enhance the separation of the photogenerated electron-hole pairs and hence improve the photocatalytic activity and change the selectivity of the reaction [10–14]. Noble metals in particular, e.g. Pt, Pd, Au, Ag, and Rh, can act as electron sinks that promote multi-electron transfer reactions that are crucial for photocatalytic efficient reduction of CO_2 [14–16]. Among those, Pt shows the highest work function (5.65 eV) and therefore lowest Fermi level and strongest electron-extracting capacity [14], and its effect as co-catalyst in CO_2 photoreduction has been the subject of a significant number of works [14,17–23]. Generally, the increased activity observed in Pt/TiO_2 catalysts compared to bare titania is ascribed to improved electron lifetime due to the mentioned ability of platinum to extract photoexcited electrons from the conduction band of TiO_2. Thus, this has been proven with photoluminescence and transient absorption spectroscopies [17,21–23], though not only for platinum but also for other metals such as silver [24], gold [25], palladium and rhodium [26]. However, platinum has shown, compared to other co-catalysts, exceptional selectivity to methane in CO_2 photoreduction [14,23] and, therefore, additional factors apart from the purely electronic ones must play a role in differentiating Pt nanoparticles, like surface chemistry and interaction with adsorbates [23,27], which on the other hand is to be expected when dealing with catalytic processes [28]. The main motivation of this work is to elucidate these additional factors that make Pt not only increase the activity of TiO_2 catalysts for CO_2 reduction, but also modify the selectivity towards highly reduce products. This would mean a significant contribution in the way towards the design of more selective photocatalytic systems for CO_2 reduction.

Another effective strategy to develop highly active photocatalysts is the construction of isolated photoactive centers in porous matrices or loading photocatalyst NPs onto zeolites or mesoporous molecular sieves. Highly dispersed Ti-oxides in silica matrices are one of the best performing photocatalysts in direct CO_2 reduction to hydrocarbons, as pioneered by Anpo and co-workers in the 1990s [29]. It is clear that the activity and selectivity of photocatalysts for different products strongly depend on the chemical nature of the supports. In brief, highly dispersed titanium dioxide in mesoporous silica materials (KIT-6, FSM-16, SBA-15 and TUD-1) leads to relatively high yields of CH_4 or/and CH_3OH, which makes it a promising candidate for CO_2 photoreduction [30]. Studies by Shioya et al. [31] and Li et al. [32] employed silica as support due to its even composition and ordered mesoporous structure with small channels. Sasirekha et al. [33] and Yang et al. [34] found that the combination of metal-doped TiO_2 with mesoporous silica enhanced the reaction rate due to effective dispersion of the photocatalyst and improved adsorption of CO_2 and H_2O on the surface of the support. Improved surface area and better dispersion of was also demonstrated for cerium Ce–TiO_2 on mesoporous silica (SBA-15) [35] in CO_2 photoreduction studies, showing that Ce–TiO_2 dispersion on the silica matrix (Ti:Si-1:4) not only improved textural properties compared to pure TiO_2, but also resulted in an order of magnitude increase in CO and CH_4 production. The adsorption properties of silica resulting from its unique mesoporous structure was one of the contributing factors due to the increased localized CO_2 concentration near the TiO_2 surface where photocatalysis could occur.

The goal of this work is therefore to shed light on the role of platinum nanoparticles acting as co-catalyst for TiO_2-photocatalyzed CO_2 reduction, aided by a high-surface mesoporous support. For that purpose, platinum has been deposited on a composite of commercial TiO_2 (Degussa P25) and COK-12 as ordered mesoporous silica material. Different Pt loadings with and without the COK-12 have been prepared, fully characterized and tested in a gas-phase photoreactor. In addition, selected samples have been characterized *in situ* with near ambient pressure x-ray photoelectron spectroscopy (NAP-XPS) and after reaction using attenuated total reflection Fourier transform infrared spectroscopy (ATR-FTIR). Special attention has been paid to the reaction pathways behind the improved selectivity towards methane production against the formation of CO mainly observed on bare titania.

2. Experimental

2.1. Preparation of photocatalysts

2.1.1. Synthesis of ordered mesoporous silica (COK-12)

Ordered mesoporous silica COK-12 was prepared as described elsewhere [31]. The synthesis takes place at room temperature. In a typical synthesis, 100 g of triblock copolymer P123 were dissolved in 2687.5 mL deionized water. After complete P123 dissolution, 92.1 g anhydrous citric acid and 63.5 g trisodium citrate dehydrate were added to control the synthesis pH between 4 and 5. The buffered surfactant solution was then stirred with overhead mechanical stirring for 24 h. A solution of 260 g sodium silicate and 750 mL deionized water was prepared and incorporated into the buffered micellar solution. Immediate solid formation was observed, and stirring was maintained for 5 min after which the slurry was kept for 24 h without stirring. The solid was separated from the mother liquor by vacuum filtration and thoroughly washed with deionized water, and then dried at 60 °C overnight. The dry solid was then calcined at 500 °C for 8 h, with a 1 °C/min heating ramp to completely remove the organic templating agent.

2.1.2. Preparation of Pt/TiO_2 photocatalysts

Pt/TiO_2 photocatalysts containing different platinum percentages were prepared by a deposition–precipitation method, according to the one initially developed by Haruta and co-workers [36]. In this procedure, different solutions were prepared, containing the appropriate amounts of the Pt precursor in 300 mL of milli-Q water. The pH of the solutions was adjusted to 9 by addition of a 0.1 M solution of NaOH. Once the pH value was stable, 2 g of TiO_2 (P25, Evonik) were added under vigorous stirring. The deposition–precipitation procedure was done at 70 °C, maintaining the pH constant during 2 h, and then the slurry was stirred overnight. The catalysts were washed and dried at 80 °C under vacuum overnight. Samples were labeled as XPt/TiO_2, where X indicates the platinum loading determined by ICP-OES in wt. %.

2.1.3. Preparation of Pt/TiO_2-COK-12 photocatalysts

Firstly, a titania sol was prepared according to the patented procedure [37] described also in our previous article [38]. Titanium isopropoxide (TTIP, 0.0492 mol) in ethanolic solution was hydrolyzed by acidic ($HClO_4$) aqueous solution. The resulting mixture was refluxed for 48 h. After such a prolonged refluxing, a stable stock of nanocrystalline titania sol was obtained. Separately, a homogeneous silica sol was prepared from TEOS (0.017 mol), de-ionized water (0.11 mol) and HCl (0.183 mmol), to hydrolyze silica precursor for later condensation reactions. The nanocrystalline titania sol (4.2 mL), the silica sol (600 mL), Levasil 200/30% (1 mL), and absolute ethanol (4 mL) were gradually mixed together to give a binder sol. Finally, a mixture of XPt/TiO_2 and COK-12 in 1:1 wt. proportions was suspended in the binder sol. The suspension was then placed in a cold ultrasonic bath for 10 min which promotes the infiltration of nanoparticles into the mesopores [39]. It is important to mention that the amount of titanium (TTIP) in the titania/binder sol suspension is 0.0081 mol while the amount of commercial titania (P25) is 0.05 mol. It has been shown in previous studies that the

effect of titania from TTIP in the titania/binder sol suspension is very low compared with commercial titania, acting only as a binder component [38]. Samples were labeled as XPt/TiO_2-COK-12, where X is the same as that in the corresponding XPt/TiO_2 sample.

2.2. Characterization

2.2.1. Characterization of COK-12

Long-range ordering of the ordered mesoporous silica COK-12 was studied by small-angle X-ray diffraction (SAXRD) in a Bruker AXS D8 ADVANCE with a Bragg–Brentano geometry and a Lynx Eye 1D detector with CuKα radiation (Bruker, Germany). Measurements were carried out between 0.5 and 6.0° 2θ value, with a step time of 1 s/0.0003° at 35 kV and 40 mA and with a 280 mm sample-detector distance. The patterns were analyzed using the Diffrac-Plus/EVA software from Bruker AXS. The pore structure, pore size and specific surface area were studied with nitrogen sorption analysis in a QuadraSorb Station 4 apparatus (Quantachrome, USA). Isotherms were recorded at 77 K after degassing the samples for 10 h at 200 °C under vacuum. The surface area was determined using the Brunauer, Emmet and Teller (BET) method [40]. The estimation of the pore size was based on NLDFT calculations using the adsorption branch of the isotherm. All nitrogen sorption data were analyzed using the Quantachrome/QuadraWin software.

2.2.2. Characterization of Pt/TiO_2 and Pt/TiO_2-COK-12 photocatalysts

The crystalline phases of synthesized photocatalyst powders were examined by XRD. The XRD patterns were obtained on a Bruker D8 Advance using Cu Kα radiation in the range between 10 and 80° with a step size of 0.034°. The diffraction patterns were analyzed using Rietveld refinement to determine the anatase average crystallite sizes. Sample displacement and zero error have been taken into account. The Brunauer–Emmett–Teller (BET) surface area of the powder specimen were calculated from the nitrogen adsorption–desorption isotherms at 77 K, using a Micromeritics-Gemini chemisorption system. The diffuse reflectance UV–vis absorption spectra were measured using a UV–vis spectrophotometer equipped with an integrating sphere (LAMBDA 650 UV/Vis with 150 mm integrating sphere, Perkin Elmer, USA). Indirect band-gap energies were determined from Tauc plots [41]. TEM images were obtained in a JEOL 7401 F microscope operated at 300 kV and at a working distance of 9 mm. The concentration of Pt in the catalyst was measured by inductively coupled plasma optical emission spectrometry (ICP-OES, Varian Inc., USA). To dissolve the platinum, a microwave method (Discover SP-D, CEM, USA) was used. Calibration of the setup was done with a commercial Pt standard solution. FTIR spectra of used catalysts were recorded on a Nicolet 6700 spectrometer (Thermo-Scientific, USA) with an ATR accessory and a DTGS detector, accumulating 32 scans with a resolution of 4 cm^{-1}. Spectra were collected at room temperature taking the naked fiber glass support as blank spectrum.

NAP-XPS spectra were acquired at the CIRCE beamline of ALBA Synchrotron, Spain. The photon energy range is 90–2000 eV and the hemispherical electron energy analyzer is a Phoibos NAP150 from SPECS that can operate at sample pressures ranging from ultra-high vacuum (UHV) up to 20 mbar. The photon energy used for the measurements was 620 eV. Photon energy calibration was done using the Au 4f level measured in a gold foil. High resolution scans (Ti2p, Pt4f, C1 s and O1 s) were acquired using 10 eV pass energy and 0.1 eV step size. The overall energy resolution was 225 meV. Samples were analyzed under sequential conditions: UHV, $CO_2 + H_2O$ atmosphere (7:1 molar ratio, total pressure 0.05 mbar) in the dark, $CO_2 + H_2O$ under UV (Hamamatsu high power UV LED centred at 365 nm), and $CO_2 + H_2O$ in the dark after reaction. Ultrapure water (LC–MS CHROMASOLV® grade, Sigma-Aldrich) was introduced into the chamber through a variable high precision leak valve after being degassed by multiple freeze − pump − thaw cycles. CO_2 (purity ≥ 99.995%, Abelló Linde) was introduced into the chamber directly from a commercial cylinder. The experiments were performed in "static mode", i.e. the analysis chamber was only pumped through the analyser entrance and through the photons entrance. Casa XPS software was used for data analysis. Shirley or two-point linear background subtractions were employed depending on the background shape. Peaks were fitted using GL(30) lineshapes. Known binding energies were used for charge correction: C1 s spectra to adventitious hydrocarbon (285 eV) [42] and Ti2p and O1 s spectra to the TiO_2 characteristic signals measured by Diebold and co. (459.3 eV and 530.4 eV respectively) [43].

2.3. Photocatalytic CO_2 reduction

Gas-phase CO_2 photoreduction experiments were conducted in continuous-flow mode in a stainless steel reactor with an effective volume of 280 mL and provided with a borosilicate window for irradiation. A suspension of 100 mg of powdered catalyst was deposited on a glass microfiber filter, dried at 100 °C under vacuum and fitted inside the reactor. UV illumination was carried out using four 6 W lamps with a maximum wavelength at 365 nm and an average irradiance of 71.7 W/m^2. Pure CO_2 and water were fed into the reaction system with a CO_2:H_2O molar ratio of 7.25 using a Controlled Evaporation and Mixing (CEM) unit. The reaction conditions were set at 2 bar and 50 °C. The products of the reaction were determined on-line by a gas chromatograph (GC Bruker 450) equipped with two separation branches and two sampling loops. The first separation branch was equipped with two semicapillary columns (BR-Q Plot and BR-Molesieve5A). This branch was also equipped with a Thermal Conductivity Detector (TCD), a Flame Ionization Detector (FID) and a methanizer. The second separation branch consisted on a capillary column (CP-Sil5B) and a second Flame Ionization Detector (FID).

Before starting the experiments, the reactor was firstly vacuumed at 50 °C and then purged with Ar (100 mL/min) for 1 h in order to remove any residual organic compounds weakly adsorbed to the surface of the catalyst. Then, CO_2 and H_2O were flowed in the dark for 1 h to establish an adsorption–desorption balance at the reaction temperature. Prior to illumination, the reactor was pressurized and kept at a reaction flow rate of 2 mL/min for another 1 h. All photocatalytic tests were carried out for 18 h. Control experiments under inert atmosphere (Ar) were performed following the same procedure and under the same conditions described above. The quantum yield index (QYI) was calculated as the ratio between the apparent quantum yield (AQY) with the corresponding sample and that with bare TiO_2 [24]:

$$QYI = \frac{AQY_{catalyst}}{AQY_{TiO2}} \quad (1)$$

$$AQY = \frac{\sum (product\ formation\ rate \times e^{-}\ implied)}{photon\ flux} \quad (2)$$

3. Results and discussion

3.1. Structural, textural and surface characteristics of the photocatalysts

The ordered mesoporous COK-12 was characterized via small-angle X-ray diffraction (SAXRD) and nitrogen adsorption (Fig. 1). The SAXRD pattern revealed three well-resolved diffraction peaks that are indexed as (100), (110) and (200) and correspond to a *P6mm* hexagonal symmetry [44]. Nitrogen sorption analysis revealed type IV isotherms with type H1 hysteresis, characteristic of materials with open cylindrical mesopores with a narrow pore size distribution, confirmed by the steep adsorption-desorption branches [45,46]. The BET surface area is 621.3 m^2/g and the mean pore size distribution determined by NLDFT is 6.1 nm, with a pore volume of 0.55 cm^3/g. All analytical results confirm the characteristics of COK-12 materials [47–49].

The X-ray diffractograms (Fig. 2) of Pt/TiO_2 and Pt/TiO_2-COK-12

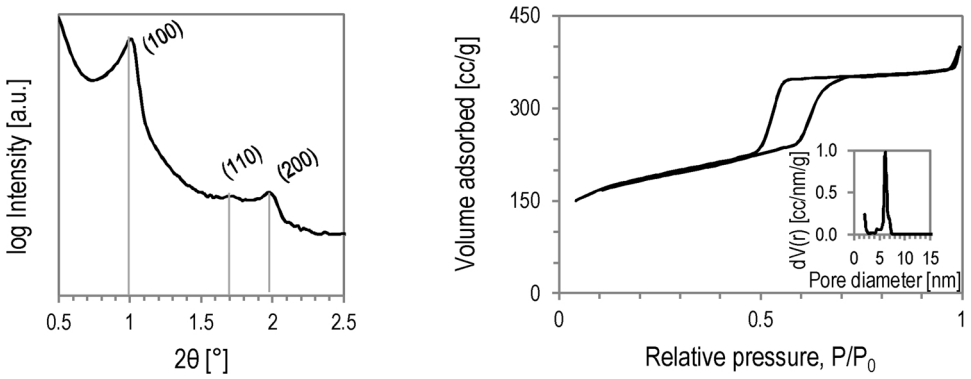

Fig. 1. Left: Small-angle XRD pattern of as-calcined COK-12 revealing 3 characteristic reflections of a hexagonal symmetry. Right: nitrogen adsorption isotherm of as-calcined COK-12. Inlet: pore size distribution determined by NLDFT.

photocatalysts confirmed that they contained anatase and rutile phases as it is well known for P25 TiO_2 [50]. The crystallite sizes of anatase (Table 1) are also in good accordance with previously reported values [50]. The slight deviations observed for the different samples must correspond to the determination uncertainty rather than to actual differences which are not to be expected from the described synthetic protocols. No Pt species were detected in XRD diagrams, which may be traced back to an ultrafine dispersion of Pt nanoparticles on TiO_2 and/or its low Pt content in the samples as measured by ICP –OES (Table 1).

The specific surface areas of as-prepared photocatalysts are summarized in Table 1. The pure TiO_2 has the lowest surface area of 55.0 $m^2 g^{-1}$. Loading with Pt increases the surface area to around 65.7 $m^2 g^{-1}$ for the largest platinum amount. It was reported that deposition of Pt nanoparticles increases the surface area of TiO_2 nanoparticles [19], which may be related to the small size of Pt nanoparticles. COK-12 has a large surface area of originally 621.3 $m^2 g^{-1}$, which decreases in the samples containing titania. The effect of Pt loading on surface area can be also observed in the Pt/TiO_2-COK-12 catalysts. Regarding indirect band-gap energies of the as-prepared samples, as expected, no significant deviations from the value of 3.1 eV determined for titania from Tauc plots (Supplementary Data, Fig. S1) are observed upon deposition of Pt or incorporation of silica.

The TEM images of samples 0.5 Pt/TiO_2 and 2 Pt/TiO_2 are shown in Fig. 3. As it can be seen, Pt nanoparticles are spread all over the titania particles. The increased amount of Pt nanoparticles on the titania surface when moving from ca. 0.5 to ca. 2 wt.% loading is evident from the images. But still the Pt nanoparticles are finely dispersed over the whole TiO_2 support with particle sizes of around 0.5 to 1 nm. Fig. 3 also shows the morphology of 0.5 Pt/TiO_2-COK-12 with low and high magnification, the former revealing that COK-12 has one-dimensional channels of ordered pores that are clearly identified. The pore size as determined by

Table 1
Main characteristics of the synthesized photocatalysts.

Sample	Anatase crystallite size (nm)	S_{BET} (m^2/g)]	Pt content [a]
TiO_2	19	55	–
TiO_2-COK-12	19	205	–
COK-12	–	621	–
0.1 Pt/TiO_2	20	55	0.13 %
0.5 Pt/TiO_2	20	56	0.58 %
2 Pt/TiO_2	21	66	2.39 %
0.1 Pt/TiO_2-COK-12	16	207	0.13 %
0.5 Pt/TiO_2-COK-12	17	216	0.58 %
2 Pt/TiO_2-COK-12	20	226	2.39 %

[a] Weight percentage with respect to TiO_2 after Pt/TiO_2 synthesis.

TEM is around 5.4 nm, in good accordance to N_2 adsorption results. In this sample, it can be seen that Pt/TiO_2 is dispersed on the surface and possibly inside the pore walls. However, the fraction of TiO_2 nanoparticles embedded in the pores of COK-12 is difficult to measure. The Pt/TiO_2 particles may block a portion of pores, which explains why the measured surface area of the samples containing Pt/TiO_2 is smaller than that of pure COK-12. Aggregates of Pt/TiO_2 on the outer surface of COK-12 are shown in the high-magnification image of 0.5 Pt/TiO_2-COK-12. Clear lattice fringes of TiO_2 as well as finely dispersed Pt nanoparticles in size of around 0.5 to 1 nm can be observed.

3.2. Photocatalytic reduction of CO_2

Fig. 4 shows the accumulated amounts of the main reaction products over 16 h of irradiation. TiO_2 led mainly to the formation of CO, together with H_2 resulting from the parallel reduction of water,

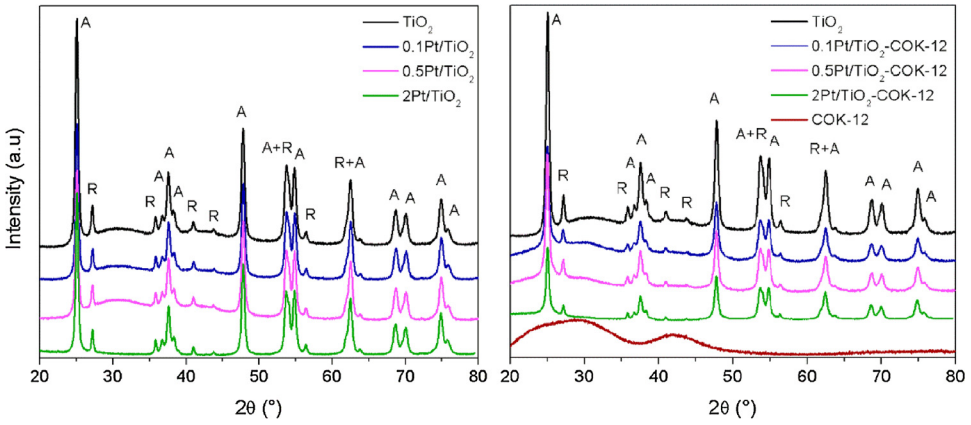

Fig. 2. XRD patterns of Pt/TiO_2 and Pt/TiO_2-COK-12 with different Pt loading. Labels A and R stand for anatase and rutile phases, respectively.

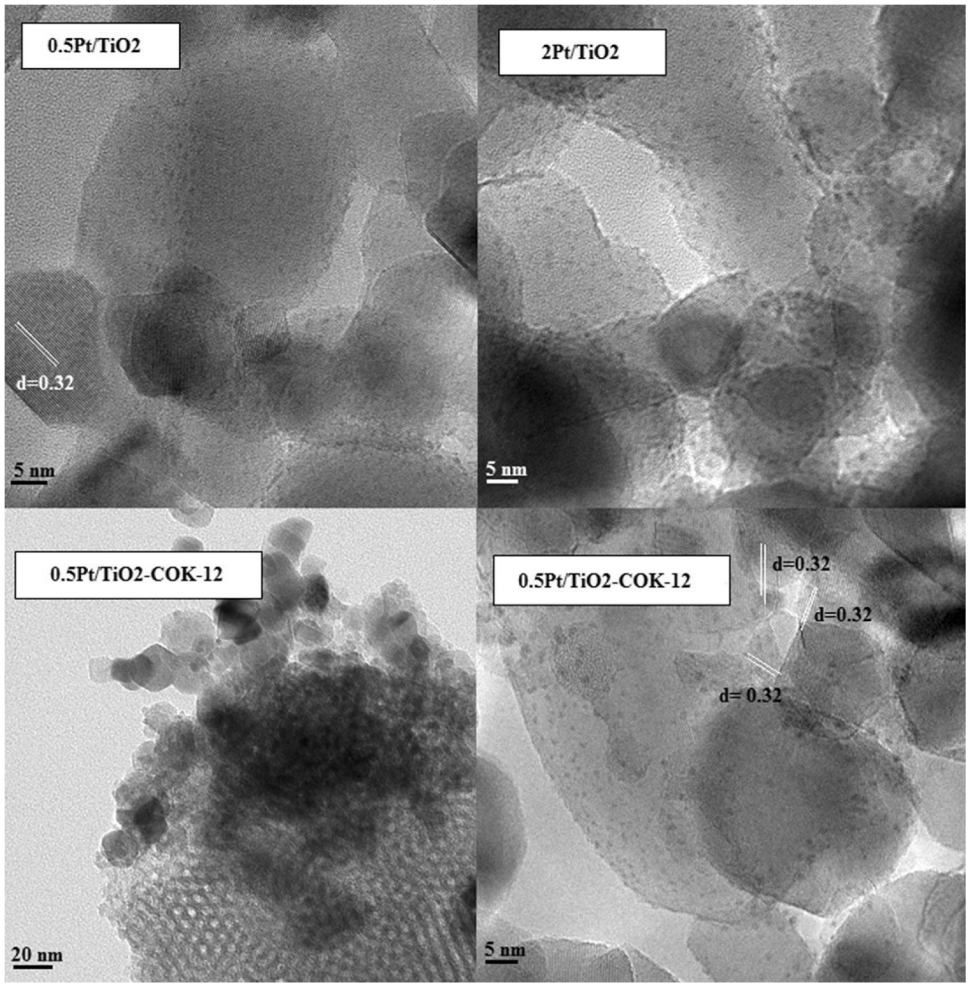

Fig. 3. TEM images of 0.5 Pt/TiO_2, 2 Pt/TiO_2 and 0.5 Pt/TiO_2-COK-12.

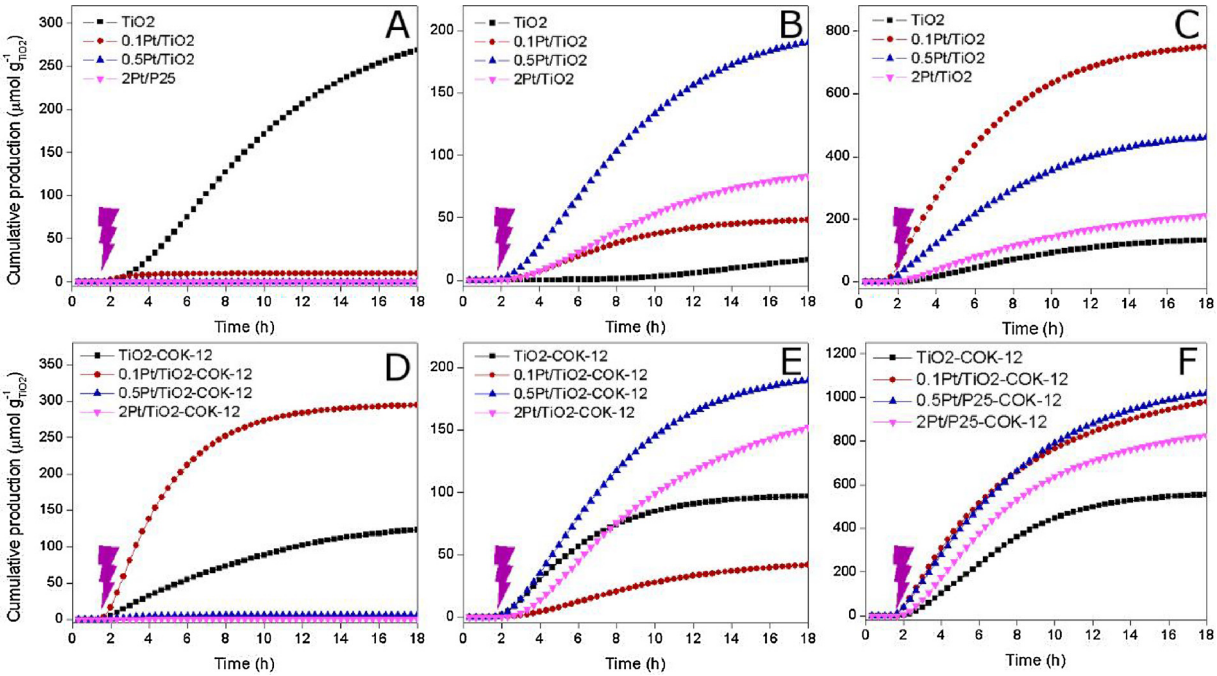

Fig. 4. Evolution of the main products obtained in the photocatalytic reduction of CO_2: CO (A, D), CH_4 (B, E), H_2 (C, F), over unsupported (A, B, C) and COK-12-supported (D, E, F) Pt/TiO_2 catalysts.

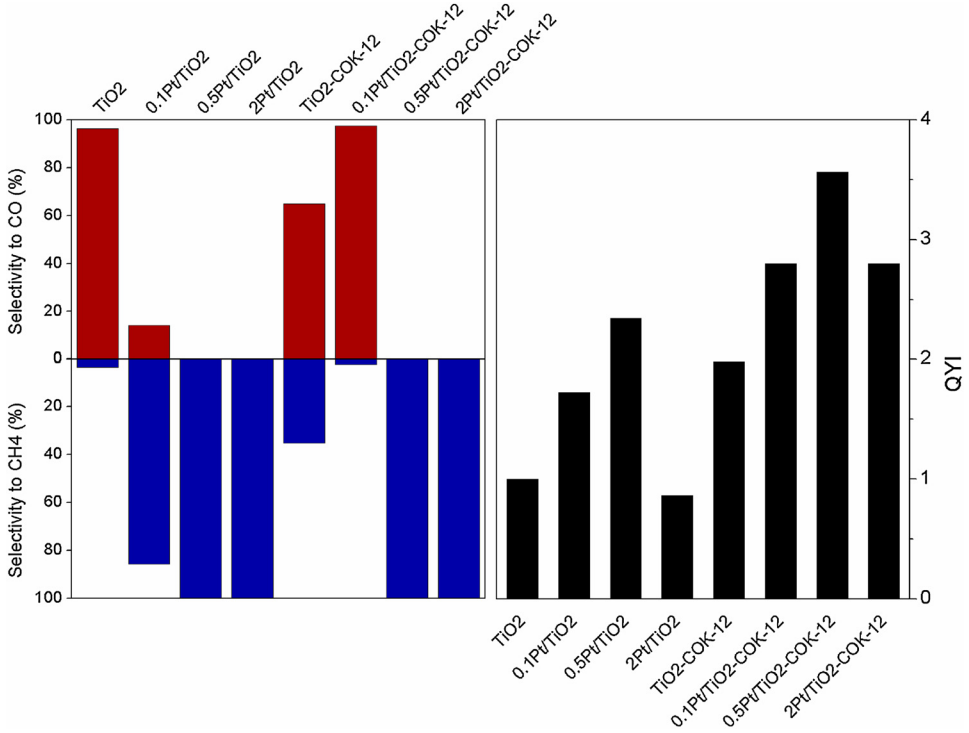

Fig. 5. Net selectivities and quantum yield indices (QYI) obtained with the different catalysts. The QYI with TiO_2 is 1 by definition.

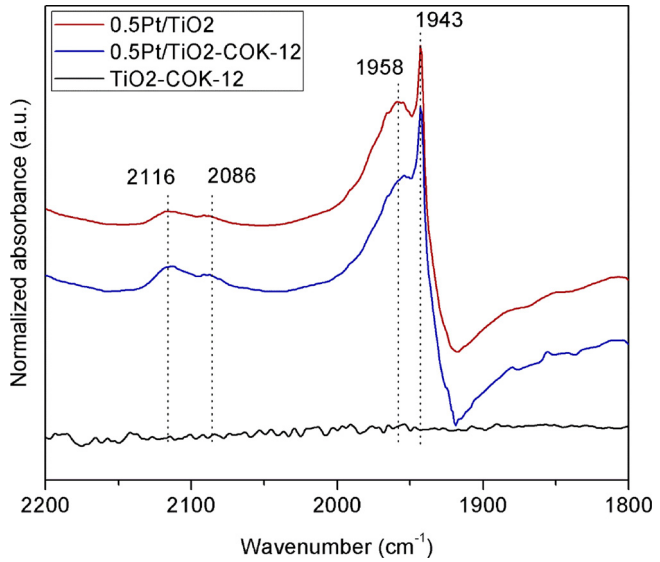

Fig. 6. ATR-FTIR spectra of the 0.5 Pt/TiO_2 and 0.5 Pt/TiO_2-COK-12 catalysts after reaction, in the CO stretching region.

competing with CO_2 for conduction band electrons. Methane was formed in a minor amount, and so was methanol (Fig. S2). Traces of other minor products like ethanol and C_2 hydrocarbons were also detected. The introduction of Pt drastically changed the situation, largely promoting the formation of methane at the expense of carbon monoxide, as well as the evolution of hydrogen, which could be expected taking into account the catalytic properties of Pt for photocatalytic hydrogen evolution [51]. Thus, the deposition of 0.13 wt.% of platinum resulted in a considerably larger CH_4 production and smaller CO evolution, which upon increasing the Pt amount to 0.58% and 2.39% turned into practically 100% selectivity to CH_4, the former producing a larger overall amount of this molecule. As described in the introduction, some works had already reported that loading of Pt lowered the recombination rate of photogenerated electron-hole pairs and improved the photocatalytic reduction efficiency of CO_2 to methane, with an optimum loading of metal above which shading effects or excessive surface coverage occur [17–23].

Similar results were observed in the case of the Pt/TiO_2-COK-12 catalysts, in which nevertheless the effect of Pt was diluted after supporting on COK-12 when it was present in only 0.13 wt.% with respect to titania, but reached a maximum in CH_4 production and selectivity with 0.58 wt.% as in the case of the unsupported catalysts. Among all the studied samples methanol production varied only within 10% with the different samples (Fig. S2), revealing a negligible effect of both the support and the co-catalysts on this product.

Irradiation experiments with P25 in an inert atmosphere (Ar) revealed that most of the CH_4 production (ca. 75%) arose from carbon residues on the catalyst surface. In the case of the TiO_2-COK-12 catalyst, notwithstanding that organic residues from the synthesis procedure of the SiO_2 support are likely contributing to carbon product formation [52], the amount of CH_4 in inert atmosphere decreased to 50% that found when CO_2 and H_2O are fed to the reactor. Therefore, the data shown in Fig. 4 partially account for reaction of the carbonaceous species on the surface of the catalysts. Remarkably, in the case of the platinum-containing catalysts this contribution is in no case larger than 30 % except for the case of the non-methane-selective 0.1 Pt/TiO_2-COK-12, revealing that these catalysts are indeed selectively reducing CO_2 to CH_4. After the contributions of the reaction under inert atmosphere have been subtracted, the selectivities between CO and CH_4 and the quantum yield indices shown in Fig. 5 are attained.

It can be concluded that the appropriate Pt content can improve the photocatalytic CO_2 reduction towards CH_4 formation as it was already reported [17–23] and, furthermore, that the selectivity can reach ca. 100% when at least 0.5 wt.% Pt with respect to TiO_2 is deposited on the surface of the catalyst. Supporting these Pt/TiO_2 catalysts on mesoporous SiO_2 (COK-12) keeps the CH_4 selectivities at these Pt loadings and, as revealed by QYI values, further improves the overall photocatalytic activity of the Pt/TiO_2 materials, which can be related to the additional effect of increased surface area and titania dispersion [30–35]. These properties are optimum in the case of the 0.5 Pt/

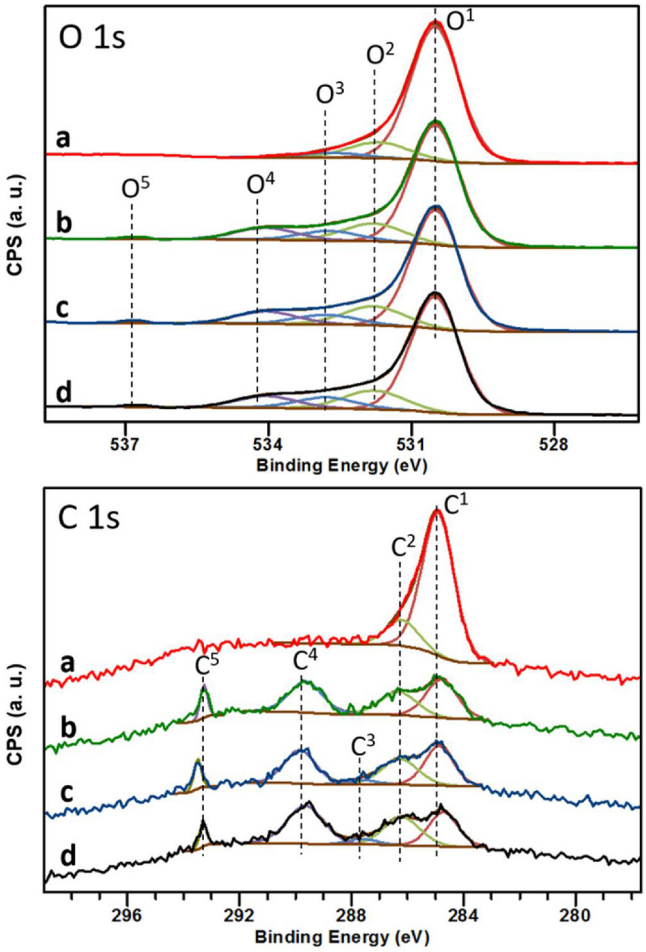

Fig. 7. O1 s and C1 s high resolution XPS spectra of 0.5 Pt/TiO_2 under sequential conditions: (a) UHV (b) 0.05 mbar CO_2:H_2O 7:1 in the dark (c) 0.05 mbar CO_2:H_2O 7:1 under UV (d) 0.05 mbar CO_2:H_2O 7:1 in the dark after reaction.

TiO_2 − COK-12 catalyst.

3.3. Spectroscopic surface studies of the CO_2 reduction pathway

In order to gain further insight into the reaction pathways leading to the observed selectivity to CH_4 in the present samples, FTIR spectra in ATR mode were recorded on the catalysts after reaction, as depicted in Fig. 6 using the optimum 0.5 Pt catalysts as example.

No features are observed in the CO stretching region on the P25-COK-12 sample, revealing negligible contribution to CO adsorption of these two components. In the case of the Pt-COntaining catalysts, however, peaks associated to CO chemisorbed on Pt are observed. Thus, the signals at 2086 and 2116 cm^{-1} can be assigned to CO molecules linearly bound to Pt° and Ptδ^+ sites, respectively [53–56]. In addition, bands at wavenumbers as low as 1958 and 1943 cm^{-1}, like the ones observed in Fig. 6, have been ascribed to CO chemisorbed on Pt sites with exceptional electron donating properties strongly interacting with the support, and tentatively assigned to Ti^{3+}-Pt-CO species [55,57]. The presence of these CO signals after reaction in the here reported catalysts may therefore be an indication of the existence of highly reducing sites able to promote the strong adsorption and further reduction of CO to CH_4.

In order to shed light onto this CO-Pt interaction, NAP-XPS measurements on a 0.5 Pt/TiO_2 sample were conducted under irradiation in a $CO_2 + H_2O$ atmosphere, following the sequence described in the experimental section. The survey scan of the sample at UHV (Fig. S3) shows the presence of all expected elements (O, Ti, Pt and C). No other elements appear after varying the experimental conditions (Fig. S2). The Ti2p region (Fig. S4) displays the typical spectrum of TiO_2 [43] without perceptible changes during the experiment (Fig. S5). A similar observation can be made regarding the Pt4f spectra (Fig. S6), in which shoulders assigned to Ptδ^+ species [58] appear at the high energy side of the main $4f_{7/2}$ and $4f_{5/2}$ peaks of metallic Pt [42] centered at 71.1 and 74.5 eV, respectively. These signals do not experience significant changes neither when varying the ambient conditions nor during or after the photocatalytic reaction (Fig. S7). In this respect, the main signals and shoulders mentioned above would hide contributions from Pt atoms bound to chemisorbed species such as CO or carbonyl species [59]. The O1 s and C1 s high resolution scans acquired under the sequential experimental conditions are shown in Fig. 7. At ultra-high vacuum, the main contribution to the O1 s signal (O^1 component in the fitting of Fig. 7) comes from the oxygen atoms within TiO_2 and has been charge corrected to the reference value of 530.4 eV [43]. Two smaller components O^2 (531.7 eV) and O^3 (532.7 eV) are observed, which have been fitted with relatively large FWHM given the different potential contributions to the peaks. Component O^2 would contain a small contribution from an unidentified signal intrinsic to the TiO_2 structure and a larger one from OH groups adsorbed on the bridging sites of the TiO_2 structure [60,61], while O^3 is assigned to the characteristic signal of terminal OH groups on the TiO_2 surface [61]. The binding energies of O^2 and O^3 components, however, could also be compatible with adsorbed CO_2 and carbonate species [62,63], or even with different CO adsorption modes on Pt [64,65]. Indeed, these two components increase their contribution to the spectrum upon introduction of CO_2 and H_2O in the chamber and further augment with UV irradiation. These components remain in the spectrum when the UV irradiation is turned back off, which confirms that the elements contributing to these peaks are from compounds that remain at the surface and may therefore be

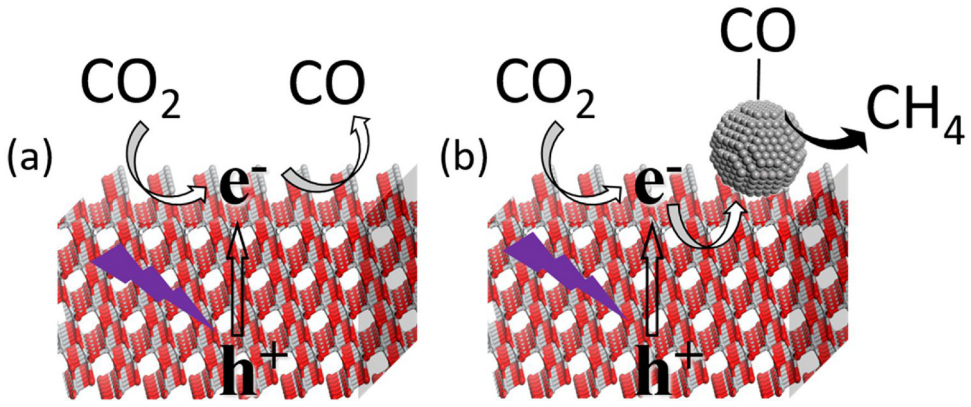

Fig. 8. Schematic representation of the proposed reaction pathway over (a) TiO_2 and (b) Pt/TiO_2 catalysts.

related to the chemisorption of these species. Additionally, two new signals O^4 (533.8 eV) and O^5 (536.7 eV) appear when CO_2 and H_2O are present. The first of them is assigned to water adsorbed on TiO_2 [60,61] and the second one has been identified as CO_2 gas by retracting the sample from the analysis spot and analyzing only the gas phase. In accordance with the reaction results, no gas-phase CO is observed in either the O1 s or the C1 s spectra [63]. The C1 s region in UHV conditions shows, in addition to the signal at 285 eV identified as adventitious aliphatic carbon (C^1 component in the fitting of Fig. 7), a second C^2 contribution at 286.2 eV that can be related to C-OH and related species [42]. In line with the O 1 s spectra, two new signals appear in the presence of CO_2 and H_2O: C^4 at 289.6 eV, assigned to surface carbonate species [62,63], and C^5 at 293.4 eV, identified as gas-phase CO_2 by retracting the sample from the analysis spot. Upon UV irradiation, the relative contribution of the C^2 component increases by ca. 25% and a shoulder appears in its high-energy side, which has been fitted as C^3 (287.2 eV). These two effects are maintained even after UV irradiation ceases. In this respect, the small increase in the C^2 component could be related to chemisorbed CO in bridging mode [64,66,67], while the C^3 component binding energy is characteristic of single-site adsorbed carbon monoxide [64,66] and surface formate [62].

In-situ NAP-XPS observations both in the O 1 s and C 1 s region are compatible, in addition to the formation of carbonate species on the surface of TiO_2 in contact with CO_2 and water [68,69], with a strong chemisorption of CO, as inferred from the ATR spectra, or even formate species, in the presence of TiO_2-supported Pt nanoparticles. This strong adsorption could promote the total reduction of CO_2 into CH_4 as observed in the photocatalytic tests, preventing CO from being the main product as it is the case for bare TiO_2, either unsupported or supported onto mesoporous silica. This proposed reaction pathways in the presence and absence of Pt is schematically depected in Fig. 8.

4. Conclusion

Pt/TiO_2 and Pt/TiO_2-COK-12 photocatalysts have been synthesized by a deposition-precipitation method. In photocatalytic CO_2 reduction over these samples in a continuous flow photoreactor, H_2, CH_4 and CO are detected as major products in all cases. While carbon monoxide is the main product obtained over TiO_2 regardless of the presence of the COK-12 as a mesoporous support. The addition of Pt leads to CO_2 reduction towards CH_4 formation, with a selectivity that reaches *ca.* 100% at optimum platinum loadings. Supporting the Pt/TiO_2 photocatalysts on COK-12 preserves the CH_4 preferential selectivity and further improves the overall activity of the Pt/TiO_2 materials. After-reaction ATR-IR and *in-situ* NAP-XPS spectra suggest a strong adsorption of CO on highly electron donating Pt sites that favours total reduction to methane.

Acknowledgements

The work was supported by the Federal Ministry of Education and Research of Germany under the "CO2Plus funding measure - Use of CO_2 to broaden the raw material basis" under the grant number 033RC003, by the International Postdoc Initiative (IPODI) of the European Union and by the Spanish Ministry of Science, Innovation and Universities through the projects *SOLPAC* (ENE2017-89170-R) and *Ra-Phuel* (ENE2016-79608-C2-1-R). Support from the Repsol Technology Centre is gratefully acknowledged. The authors would like to thank the assistance of ALBA staff for the measurements at the CIRCE beamline from the ALBA Synchrotron Light Source. We would like to thank Christina Eichenauer and Maria Unterweger from TU Berlin for nitrogen sorption and SAXRD measurements.

Appendix A. Supplementary data

Supplementary material related to this article can be found, in the online version, at doi:https://doi.org/10.1016/j.apcatb.2018.08.003.

References

[1] T.J. Blasing, Recent Greenhouse Gas Concentrations, Carbon Dioxide Inf. Anal. Center, Oak Ridge Natl. Lab., 2009, pp. 1–5, https://doi.org/10.3334/CDIAC/atg.032.
[2] D.Y.C. Leung, X. Fu, C. Wang, M. Ni, M.K.H. Leung, X. Wang, X. Fu, Hydrogen production over titania-based photocatalysts, ChemSusChem 3 (2010) 681–694, https://doi.org/10.1002/cssc.201000014.
[3] K. Kočí, L. Obalová, Z. Lacný, Photocatalytic reduction of CO2 over TiO2 based catalysts, Chem. Pap. 62 (2008) 1–9, https://doi.org/10.2478/s11696-007-0072-x.
[4] C. Peng, G. Reid, H. Wang, P. Hu, Perspective: photocatalytic reduction of CO $_2$ to solar fuels over semiconductors, J. Chem. Phys. 147 (2017) 030901, , https://doi.org/10.1063/1.4985624.
[5] J.K. Stolarczyk, S. Bhattacharyya, L. Polavarapu, J. Feldmann, Challenges and prospects in solar water splitting and CO $_2$ reduction with inorganic and hybrid nanostructures, ACS Catal. (2018) 3602–3635, https://doi.org/10.1021/acscatal.8b00791.
[6] T. Inoue, A. FUJishima, S. Konishi, K. Honda, Photoelectrocatalytic reduction of carbon dioxide in aqueous suspensions of semiconductor powders, Nature 277 (1979) 637–638, https://doi.org/10.1038/277637a0.
[7] L. Liu, Y. Li, Understanding the reaction mechanism of photocatalytic reduction of CO2 with H2O on TiO2-based photocatalysts: A review, Aerosol Air Qual. Res. 14 (2014) 453–469, https://doi.org/10.4209/aaqr.2013.06.0186.
[8] J. Low, B. Cheng, J. Yu, Surface modification and enhanced photocatalytic CO2 reduction performance of TiO2: a review, Appl. Surf. Sci. 392 (2017) 658–686, https://doi.org/10.1016/j.apsusc.2016.09.093.
[9] O. Ishitani, C. Inoue, Y. Suzuki, T. Ibusuki, Photocatalytic reduction of carbon dioxide to methane and acetic acid by an aqueous suspension of metal-deposited titania, J. Photochem. Photobiol. A Chem. 72 (1993) 269–271.
[10] X. Li, J. Wen, J. Low, Y. Fang, J. Yu, Design and fabrication of semiconductor photocatalyst for photocatalytic reduction of CO2 to solar fuel, Sci. China Mater. (2014), https://doi.org/10.1007/s40843-014-0003-1.
[11] S.N. Habisreutinger, L. Schmidt-Mende, J.K. Stolarczyk, Photocatalytic reduction of CO2 on TiO2 and other semiconductors, Angew. Chem. Int. Ed. 52 (2013) 7372–7408, https://doi.org/10.1002/anie.201207199.
[12] S. Bai, W. Yin, L. Wang, Y. Xiong, Surface and interface design in cocatalysts for photocatalytic water splitting and CO2 reduction, RSC Adv. 6 (2016) 57446–57463, https://doi.org/10.1039/C6RA10539D.
[13] X. Chang, T. Wang, J. Gong, CO2 Photo-reduction: Insights into CO2 Activation and Reaction on Surfaces of Photocatalysts, Energy Environ. Sci. 9 (2016) 2177–2196, https://doi.org/10.1039/C6EE00383D.
[14] J. Ran, M. Jaroniec, S.-Z. Qiao, Cocatalysts in semiconductor-based photocatalytic co2 reduction: achievements, challenges, and opportunities, Adv. Mater. 1704649 (2018), https://doi.org/10.1002/adma.201704649 1704649.
[15] V.P. Indrakanti, J.D. Kubicki, H.H. Schobert, Photoinduced activation of CO2 on Ti-based heterogeneous catalysts: Current state, chemical physics-based insights and outlook, Energy Environ. Sci. 2 (2009) 745, https://doi.org/10.1039/b822176f.
[16] H. Abdullah, M.M.R. Khan, H.R. Ong, Z. Yaakob, Modified TiO2 photocatalyst for CO2 photocatalytic reduction: an overview, J. CO2 Util. 22 (2017) 15–32, https://doi.org/10.1016/j.jcou.2017.08.004.
[17] W. Wang, W. An, B. Ramalingam, S. Mukherjee, D.M. Niedzwiedzki, S. Gangopadhyay, P. Biswas, Size and structure matter: enhanced co 2 photo-reduction efficiency by size-resolved ultra fine Pt nanoparticles on TiO2 single crystals, J. Am. Chem. Soc. 134 (2012) 11276–11281, https://doi.org/10.1021/ja304075b.
[18] Z. Xiong, Z. Lei, X. Chen, B. Gong, Y. Zhao, J. Zhang, C. Zheng, J.C.S. Wu, CO2 photocatalytic reduction over Pt deposited TiO2 nanocrystals with coexposed {101} and {001} facets: effect of deposition method and Pt precursors, Catal. Commun. 96 (2017) 1–5, https://doi.org/10.1016/j.catcom.2017.03.013.
[19] Z. Xiong, H. Wang, N. Xu, H. Li, B. Fang, Y. Zhao, J. Zhang, C. Zheng, Photocatalytic reduction of CO2 on Pt2+–Pt0/TiO2 nanoparticles under UV/Vis light irradiation: a combination of Pt2+ doping and Pt nanoparticles deposition, Int. J. Hydrogen Energy 40 (2015) 10049–10062, https://doi.org/10.1016/j.ijhydene.2015.06.075.
[20] B. Fang, A. Bonakdarpour, K. Reilly, Y. Xing, F. Taghipour, D.P. Wilkinson, Large-scale synthesis of TiO2 microspheres with hierarchical nanostructure for highly efficient photodriven reduction of CO2 to CH4, ACS Appl. Mater. Interfaces 6 (2014) 15488–15498, https://doi.org/10.1021/am504128t.
[21] J. Mao, L. Ye, K. Li, X. Zhang, J. Liu, T. Peng, L. Zan, Pt-loading reverses the photocatalytic activity order of anatase TiO2 {001} and {010} facets for photo-reduction of CO2 to CH4, Appl. Catal. B Environ. 144 (2014) 855–862, https://doi.org/10.1016/j.apcatb.2013.08.027.
[22] Y. Wang, Q. Lai, F. Zhang, X. Shen, M. Fan, Y. He, S. Ren, High efficiency photocatalytic conversion of CO2 with H2O over Pt/TiO2 nanoparticles, RSC Adv. 4 (2014) 44442–44451, https://doi.org/10.1039/C4RA07457B.
[23] S. Xie, Y.Y. Wang, Q. Zhang, W. Deng, Y.Y. Wang, MgO- and Pt-promoted TiO2 as an efficient photocatalyst for the preferential reduction of carbon dioxide in the presence of water, ACS Catal. 4 (2014) 3644–3653, https://doi.org/10.1021/cs500648p.
[24] L. Collado, P. Jana, B. Sierra, J.M. Coronado, P. Pizarro, D.P. Serrano, V.A. de la Peña O'Shea, Enhancement of hydrocarbon production via artificial photosynthesis due to synergetic effect of Ag supported on TIO2 and ZnO semiconductors, Chem. Eng. J. 224 (2013) 128–135, https://doi.org/10.1016/j.cej.2012.12.053.
[25] L. Collado, A. Reynal, J.M. Coronado, D.P. Serrano, J.R. Durrant, V.A. de la Peña

O'Shea, Effect of Au surface plasmon nanoparticles on the selective CO2 photoreduction to CH4, Appl. Catal. B Environ. 178 (2015) 177–185, https://doi.org/10.1016/j.apcatb.2014.09.032.
[26] Y. Zhu, Z. Xu, Q. Lang, W. Jiang, Q. Yin, S. Zhong, S. Bai, Grain boundary engineered metal nanowire cocatalysts for enhanced photocatalytic reduction of carbon dioxide, Appl. Catal. B Environ. 206 (2017) 282–292, https://doi.org/10.1016/j.apcatb.2017.01.035.
[27] X. Feng, J.D. Sloppy, T.J. LaTempa, M. Paulose, S. Komarneni, N. Bao, Ca. Grimes, Synthesis and deposition of ultrafine Pt nanoparticles within high aspect ratio TiO2 nanotube arrays: application to the photocatalytic reduction of carbon dioxide, J. Mater. Chem. 21 (2011) 13429, https://doi.org/10.1039/c1jm12717a.
[28] K. Takanabe, Photocatalytic Water Splitting: Quantitative Approaches toward Photocatalyst by Design, ACS Catal. 7 (2017) 8006–8022, https://doi.org/10.1021/acscatal.7b02662.
[29] H. Yamashita, A. Shiga, S. ichi Kawasaki, Y. Ichihashi, S. Ehara, M. Anpo, Photocatalytic synthesis of CH4 and CH3OH from CO2 and H2O on highly dispersed active titanium oxide catalysts, Energy Convers. Manag. 36 (1995) 617–620, https://doi.org/10.1016/0196-8904(95)00081-N.
[30] M. Anpo, Photocatalytic reduction of CO2with H2O on highly dispersed Ti-oxide catalysts as a model of artificial photosynthesis, J. CO2 Util. 1 (2013) 8–17, https://doi.org/10.1016/j.jcou.2013.03.005.
[31] Y. Shioya, K. Ikeue, M. Ogawa, M. Anpo, Synthesis of transparent Ti-containing mesoporous silica thin film materials and their unique photocatalytic activity for the reduction of CO 2 with H2O, Appl. Catal. A Gen. 254 (2003) 251–259, https://doi.org/10.1016/S0926-860X(03)00487-3.
[32] Y. Li, W.-N. Wang, Z. Zhan, M.-H. Woo, C.-Y. Wu, P. Biswas, Photocatalytic reduction of CO2 with H2O on mesoporous silica supported Cu/TiO2 catalysts, Appl. Catal. B Environ. 100 (2010) 386–392, https://doi.org/10.1016/j.apcatb.2010.08.015.
[33] N. Sasirekha, S. John, S. Basha, K. Shanthi, Photocatalytic performance of Ru doped anatase mounted on silica for reduction of carbon dioxide, Appl. Catal. B Environ. 62 (2006) 169–180, https://doi.org/10.1016/j.apcatb.2005.07.009.
[34] H.-C.C. Yang, H.-Y.Y. Lin, Y.-S.S. Chien, J.C.-S.S. Wu, H.-H.H. Wu, Mesoporous TiO2/SBA-15, and Cu/TiO2/SBA-15 composite photocatalysts for photoreduction of CO2 to methanol, Catal. Lett. 131 (2009) 381–387, https://doi.org/10.1007/s10562-009-0076-y.
[35] C. Zhao, L. Liu, Q. Zhang, J. Wang, Y. Li, Photocatalytic conversion of CO2 and H2O to fuels by nanostructured Ce–TiO2/SBA-15 composites, Catal. Sci. Technol. 2 (2012) 2558, https://doi.org/10.1039/c2cy20346d.
[36] M. Haruta, T. Kobayashi, H. Sano, N. Yamada, Novel gold catalysts for the oxidation of carbon monoxide at a temperature far below 0 °C, Chem. Lett. 16 (1987) 405–408, https://doi.org/10.1246/cl.1987.405.
[37] K. Nosilcih, Z.A. Namene, F. Čiščenja, Patent, (n.d.) 1–15.
[38] M. Tasbihi, I. Calin, A. Šuligoj, M. Fanetti, U. Lavrencic Štangar, Photocatalytic degradation of gaseous toluene by using TiO 2 nanoparticles immobilized on fiberglass cloth, J. Photochem. Photobiol. A Chem. 336 (2017) 89–97, https://doi.org/10.1016/j.jphotochem.2016.12.025.
[39] N.V. Dezhkunov, T.G. Leighton, Study into correlation between the ultrasonic capillary effect and sonoluminescence, J. Eng. Phys. Thermophys. 77 (2004) 53–61.
[40] S. Brunauer, P.H. Emmett, E. Teller, Adsorption of gases in multimolecular layers, J. Am. Chem. Soc. 60 (1938) 309–319, https://doi.org/10.1021/ja01269a023.
[41] L. Yang, B. Kruse, Revised Kubelka Munk theory. I. Theory and application, J. Opt. Soc. Am. 21 (2004) 1933–1941, https://doi.org/10.1364/JOSAA.21.001933.
[42] C.D. Wagner, W.M. Riggs, L.E. Davies, J.F. Moulder, Handbook of X-ray Photoelectron Spectroscopy, Perkin-Elmer Corporation, 1979.
[43] U. Diebold, T.E. Madey, TiO2 by XPS, Surf. Sci. Spectra 227 (1996) 227–231, https://doi.org/10.1116/1.1247794.
[44] K. Holmberg, D.O. Shah, M.J. Schwuger, Handbook of Applied Surface and Colloid Chemistry, John Wiley & Sons, LTD, 2002.
[45] K.S.W. SIng, Reporting physisorption data for gas/solid systems, Pure Appl. Chem. 54 (1982) 2201–2218.
[46] M. Thommes, K. Kaneko, A.V. Neimark, J.P. Olivier, F. Rodriguez-Reinoso, J. Rouquerol, K.S.W. Sing, Physisorption of gases, with special reference to the evaluation of surface area and pore size distribution (IUPAC Technical Report), Pure Appl. Chem. 87 (2015) 1051–1069, https://doi.org/10.1515/pac-2014-1117.
[47] M.G. Colmenares, U. Simon, M. Yildiz, S. Arndt, R. Schomaecker, A. Thomas, F. Rosowski, A. Gurlo, O. Goerke, Oxidative coupling of methane on the Na2WO4-MnxOy catalyst: COK-12 as an inexpensive alternative to SBA-15, Catal. Commun. 85 (2016) 75–78, https://doi.org/10.1016/j.catcom.2016.06.025.
[48] J. Jammaer, A. Aerts, J. D'Haen, J.W. Seo, J.A. Martens, Convenient synthesis of ordered mesoporous silica at room temperature and quasi-neutral pH, J. Mater. Chem. 19 (2009) 8290, https://doi.org/10.1039/b915273c.
[49] M.G. Colmenares, U. Simon, O. Cruz, A. Thomas, O. Goerke, A. Gurlo, Batch and continuous synthesis upscaling of powder and monolithic ordered mesoporous silica COK-12, Microporous Mesoporous Mater. 256 (2018) 102–110, https://doi.org/10.1016/j.micromeso.2017.08.002.
[50] T. Ohno, K. Sarukawa, K. Tokieda, M. Matsumura, Morphology of a TiO2photocatalyst (Degussa, P-25) consisting of anatase and rutile crystalline phases, J. Catal. 203 (2001) 82–86, https://doi.org/10.1006/jcat.2001.3316.
[51] K. Maeda, K. Domen, Photocatalytic water splitting: recent progress and future challenges, J. Phys. Chem. Lett. 1 (2010) 2655–2661, https://doi.org/10.1021/jz1007966.
[52] I. Grigioni, M.V. Dozzi, M. Bernareggi, G.L. Chiarello, E. Selli, Photocatalytic CO 2 reduction vs. H2 production : The effects of surface carbon-containing impurities on the performance of TiO2 -based photocatalysts, Catal. Today 281 (2017) 214–220, https://doi.org/10.1016/j.cattod.2016.05.040.
[53] N.S. Resende, C.A. Perez, J.G. Eon, M. Schmal, The effect of coating TiO2 on the CO oxidation of the Pt/γ-alumina catalysts, Catal. Lett. 141 (2011) 1685–1692, https://doi.org/10.1007/s10562-011-0695-y.
[54] E. Ivanova, M. Mihaylov, M. Daturi, K. Hadjiivanov, FTIR spectroscopy study of CO and NO adsorption and co-adsorption on Pt/TiO2, J. Mol. Catal. A Chem. 274 (2007) 179–184, https://doi.org/10.1016/j.molcata.2007.05.006.
[55] P. Panagiotopoulou, D.I. Kondarides, Effects of alkali additives on the physicochemical characteristics and chemisorptive properties of Pt/TiO2 catalysts, J. Catal. 260 (2008) 141–149, https://doi.org/10.1016/j.jcat.2008.09.014.
[56] H. Gao, W. Xu, H. He, X. Shi, X. Zhang, K. Tanaka, Molecular and Biomolecular Spectroscopy DRIFTS investigation and DFT calculation of the adsorption of CO on Pt/TiO2, Pt/CeO2 and FeOx/Pt /CeO2, Spectrochim, Acta Part A Mol. Biomol. Spectrosc. 71 (2008) 1193–1198, https://doi.org/10.1016/j.saa.2008.03.036.
[57] P. Panagiotopoulou, A. Christodoulakis, D.I. Kondarides, S. Boghosian, Particle size effects on the reducibility of titanium dioxide and its relation to the water– gas shift activity of Pt/TiO2 catalysts, J. Catal. 240 (2006) 114–125, https://doi.org/10.1016/j.jcat.2006.03.012.
[58] H. Na, T. Zhu, Z. Liu, Effect of preparation method on the performance of Pt–Au/TiO2 catalysts for the catalytic co-oxidation of HCHO and CO, Catal. Sci. Technol. 4 (2014) 2051–2057, https://doi.org/10.1039/c4cy00020j.
[59] W.D. Michalak, J.M. Krier, S. Alayoglu, J. Shin, K. An, K. Komvopoulos, Z. Liu, G.A. Somorjai, CO oxidation on PtSn nanoparticle catalysts occurs at the interface of Pt and Sn oxide domains formed under reaction conditions, J. Catal. 312 (2014) 17–25, https://doi.org/10.1016/j.jcat.2014.01.005.
[60] M.J. Jackman, A.G. Thomas, C. Muryn, Photoelectron spectroscopy study of stoichiometric and reduced anatase TiO2 (101) surfaces: The effect of subsurface defects on water adsorption at near-ambient pressures, J. Phys. Chem. C 119 (2015) 13682–13690, https://doi.org/10.1021/acs.jpcc.5b02732.
[61] H. Perron, D.J. Vandenborre, R. Drot, J. Roques, E. Simoni, J.-J. Ehrhardt, H. Catalette, Combined investigation of water sorption on TiO2 rutile (1 1 0) single crystal face : XPS vs. periodic DFT, Surf. Sci. 601 (2007) 518–527, https://doi.org/10.1016/j.susc.2006.10.015.
[62] X. Deng, A. Verdaguer, T. Herranz, C. Weis, H. Bluhm, M. Salmeron, Surface chemistry of Cu in the presence of CO2 and H2O, Langmuir 24 (2008) 9474–9478.
[63] K. Mudiyanselage, S.D. Senanayake, L. Feria, S. Kundu, A.E. Baber, J. Graciani, A.B. Vidal, S. Agnoli, J. Evans, R. Chang, S. Axnanda, Z. Liu, J.F. Sanz, P. Liu, J.A. Rodriguez, D.J. Stacchiola, Importance of the metal – oxide interface in catalysis: in situ studies of the water – gas shift reaction by ambient-pressure X-ray photoelectron spectroscopy, Angew. Chem. Int. Ed. 52 (2013) 5101–5105, https://doi.org/10.1002/anie.201210077.
[64] M. Montano, K. Bratlie, M. Salmeron, G.A. Somorjai, Hydrogen and deuterium exchange on Pt (111) and its poisoning by carbon monoxide studied by surface sensitive high-pressure techniques, J. Am. Chem. Soc. (2006) 13229–13234, https://doi.org/10.1021/ja063703a.
[65] A.S. Duke, R.P. Galhenage, S.A. Tenney, P. Sutter, D.A. Chen, In situ studies of carbon monoxide oxidation on platinum and platinum − rhenium alloy surfaces, J. Phys. Chem. C 119 (2015) 381–391, https://doi.org/10.1021/jp509725n.
[66] R. Toyoshima, M. Yoshida, Y. Monya, K. Suzuki, K. Amemiya, K. Mase, B.S. Mun, H. Kondoh, A high-pressure-induced dense CO overlayer on a Pt(111) surface: a chemical analysis using in situ near ambient pressure XPS, Phys. Chem. Chem. Phys. 16 (2014) 23564–23567, https://doi.org/10.1039/C4CP04318A.
[67] K. Tanaka, K. Miyahara, I. Toyoshima, Adsorption of carbon dioxide on titanium dioxide and platinum/titanium dioxide studied by x-ray photoelectron spectroscopy and Auger electron spectroscopy, J. Phys. Chem. 88 (1984) 3504–3508, https://doi.org/10.1021/j150660a026.
[68] H. Zhao, L. Liu, J.M. Andino, Y. Li, Bicrystalline TiO2 with controllable anatase–brookite phase content for enhanced CO2 photoreduction to fuels, J. Mater. Chem. A 1 (2013) 8209, https://doi.org/10.1039/c3ta11226h.
[69] C.C. Yang, Y.H. Yu, B. Van Der Linden, J.C.S. Wu, G. Mul, Artificial photosynthesis over crystalline TiO2-based catalysts: Fact or fiction? J. Am. Chem. Soc. 132 (2010) 8398–8406, https://doi.org/10.1021/ja101318k.